Progress In Electromagnetics Research, PIER 94, 19–32, 2009

A TRUST REGION SUBPROBLEM FOR 3D ELECTRICAL IMPEDANCE TOMOGRAPHY INVERSE PROBLEM USING EXPERIMENTAL DATA

M. Goharian

Medical Physics and Applied Radiation Sciences
McMaster University
Hamilton, Canada

M. Soleimani

Electronic and Electrical Engineering
University of Bath
Bath, UK

G. R. Moran

Medical Physics and Applied Radiation Sciences
McMaster University
Hamilton, Canada

Abstract—Image reconstruction in electrical impedance tomography (EIT) is an ill-posed nonlinear inverse problem. Regularization methods are needed to solve this problem. The results of the ill-posed EIT problem strongly depends on noise level in measured data as well as regularization parameter. In this paper, we present trust region subproblem (TRS), with the use of L-curve maximum curvature criteria to find a regularization parameter. Currently Krylov subspace methods especially conjugate gradient least squares (CGLS) are used for large scale 3D problem. CGLS is an efficient technique when the norm of measured noise is exactly known. This paper demonstrates that CGLS and TRS converge to the same point on the L-curve with the same noise level. TRS can be implemented efficiently for large scale inverse EIT problem as CGLS with no need a priori knowledge of the noise level.

Corresponding author: M. Soleimani (m.soleimani@bath.ac.uk).

1. INTRODUCTION

Electrical impedance tomography (EIT) is a non-invasive technique that aims to reconstruct images of internal impedance values of a volume of interest, based on measurements taken on the external boundary [8, 9]. In EIT the internal electrical conductivity can be reconstructed from voltage measurements on the surface of an object under study. EIT has potential application in physiological measurement as well as industrial process monitoring.

The image reconstruction in EIT is a challenging inverse problem. In the case of complete and noiseless boundary measurements, the EIT problem is known to have a unique solution. In practice however, the measured data is noisy and incomplete. Hence, in this situation it is difficult to obtain a satisfactory solution from the nonlinear and ill-posed EIT problem. So it is necessary to use regularization techniques because of the ill-posed nature of the problem.

Each regularization method employs a special parameter, known as the *regularization parameter*, to control the effect of the noise on the solution. The nature of the regularization parameter is different for each method. For instance, in Tikhonov regularization the penalty parameter acts as regularization parameters, and in iterative approaches the number of iterations will serve as the regularization parameter [15, 16].

CGLS creates components in the direction of singular vectors related to large singular values at the early stages of iterations. While components associated with small singular values will be effective at later iterations this means that the number of iterations acts as a regularization parameter. Thus, the regularized solution would be obtained by stopping the iteration before the unwanted components added to the current solution.

The success of CGLS strongly depends on knowing when to stop the iteration, which is a difficult task in itself. On the other hand, we could use CGLS with the Tikhonov regularization approach, which is called a damped least squares problem. The convergence of this technique also depends on both a good choice of the damping parameter and a preconditioner.

In this paper, we introduce the regularization problem as a quadratic constrained least squares problem. It has been shown that this approach is equivalent to Tikhonov regularization [1]. In the area of optimization this problem is a special case of trust-region methods which is known as the trust-region subproblem [2]. A comprehensive study regarding different approaches for solving the regularization problem as a trust-region subproblem is given in [3].

We adopted the recently developed method for solving the trust-region subproblem in the regularization case [4] for the EIT problem. In this method the regularized solution was obtained using a parameterized trust region approach to estimate the region of maximum curvature of the L-curve. Method proposed here can be used in other imaging techniques [17–21].

2. THE INVERSE PROBLEM

In the EIT problem, the relation between perturbations in the internal conductivity distribution and the perturbations in the boundary measurements is nonlinear. However, this nonlinear relation can be formulated using a linearized form. If in the continuous region, J is the Fréchet derivative of the potential, U, with respect to conductivity, σ, for the nonlinear mapping $\sigma \mapsto U(\sigma)$, then the linearized form has following form

$$Jx = \delta U \tag{1}$$

where $x \in \Re^n$ is the perturbation in conductivity distribution that maps to the differential measurements $\delta U \in \Re^m$, and $J \in \Re^{m \times n}$ is the Jacobian matrix. Due to the ill-posed nature of problem, x cannot be recovered from (1). In practice, the most popular technique is to apply the conjugate gradient method to the normal equations associated with problem (1). In this way a least square conjugate gradient approach to solve the inverse problem can be implemented in a similar fashion to a least square problem

$$\min_x \|Jx - \delta U\|_2 \tag{2}$$

The regularized Gauss-Newton method is the most commonly used method for the inverse problem in EIT. In regularized Gauss-Newton method the second order term in the Hessian is approximated. The regularized optimization is to find x, given x_0 as the initial guess, Rx the regularization function; we also include regularization parameter α here, so that the cost functional is

$$g(x) = \frac{1}{2} \|\delta U - Jx\| + \alpha^2 R \tag{3}$$

For regularized Gauss-Newton the iteration steps are $x_{i+1} = x - H(x_i)^{-1} \nabla g(x_i)$, where $H(x_i) = J^T J + \alpha^2 R''(x_i)$, where H is the modified Hessian here and R is regularization function and $\nabla g(x_i) = J'(\delta U - Jx) + \alpha^2 R'(x_i)$. Here $R'(x_i)$ and $R''(x_i)$ are the first and second derivatives of $R(x_i)$ with respect to x_i.

3. TRUST REGION SUBPROBLEM

3.1. Structure of Problem

We formulate the EIT regularization problem as the following quadratically constrained least squares problem

$$\begin{aligned} R_\Delta := \quad & \min \ \|Jx - \delta U\|_2 \\ & \mathbf{s.t.} \ \|x\|_2 \leq \Delta \end{aligned} \tag{4}$$

with $\Delta > 0$. Using the method of Lagrange multipliers it was shown [1] that this formulation is equal to Tikhonov regularization. This means that any solution to (4) with the value of Δ is equivalent to solving the following Tikhonov regularization with parameter α

$$(J^T J + \alpha^2 I)x_\alpha = J^T \delta U \tag{5}$$

It gives $x_\alpha = x_\Delta$. The solutions for (4) are the same as the following problem which can be formulated by squaring both objective and constraint in (4),

$$\begin{aligned} \eta_\Delta := \quad & \min \ Q(x) := x^T H x - 2G^T x \\ & \mathbf{s.t.} \ \|x\|_2^2 \leq \Delta^2 \end{aligned} \tag{6}$$

where $H = J^T J$ and $G = J^T \delta U$. The optimization problem in (6) is called the *trust region subproblem* (TRS). The solution for the regularization problem (4) is found by solving the TRS (6) sequentially. The TRS can be used to form the *L-curve*,

$$L(J, \delta U) = \{(\log(\Delta), \log \|Jx_\Delta - \delta U\|) : \Delta > 0\} \tag{7}$$

The regularization parameter, Δ, can be found through the point of maximum curvature, or the *elbow*, on the L-*curve* [5]. Therefore, the trust region radius, Δ, needs to change iteratively to steer the algorithm to the elbow of the L-curve.

A feasible vector $x^* = x_\Delta$ is a solution to (6) if and only if [6]:

$$\begin{aligned} & (H - \lambda^* I)x_\Delta = G \\ & (H - \lambda^* I) \geq 0 \\ & \lambda^* \left(\|x_\Delta\|_2^2 - \Delta^2 \right) = 0 \\ & \lambda^* \leq 0 \end{aligned} \tag{8}$$

for a Lagrange multiplier $\lambda^* = \lambda_\Delta$. These conditions relate the Tikhonov regularization (5) to the TRS (6).

A solution x^* to the TRS (3) is a solution to (3) corresponding to $\alpha^2 = -\lambda_\Delta$

$$(H - \lambda_\Delta I)x_{\lambda_\Delta} = G \tag{9}$$

Conversely, any solution x_α to (4) for α, solves (5) for $\Delta^2 = \|x_\alpha\|_2^2$. So the objective function value in (4) and Δ represent a unique point on the L-curve.

3.2. Creation of L-curve with TRS

From [7] we know the strong Lagrangian duality is satisfied for TRS so that TRS can be formulated as an unconstrained concave maximization problem, i.e.,

$$\eta_\Delta = \max_{\lambda \le 0} \min_x L(x, \lambda) \tag{10}$$

where $L(x, \lambda) = x^T H x - 2G^T x + \lambda(\Delta^2 - \|x\|_2^2)$ represents Lagrangian of TRS. Define

$$D(t) = \begin{pmatrix} t & -G^T \\ -G & t \end{pmatrix}, \; k(t) := (\Delta^2 + 1)\lambda_1(D(t)) - t \tag{11}$$

where the $\lambda_1(D(t))$ is the smallest eigenvalue for $D(t)$. Then the unconstrained dual problem for TRS is as follows

$$\eta_\Delta = \max_t k(t) \tag{12}$$

The L-curve is formed using Δ in TRS as a parameter and finding the residual for the corresponding optimal x_Δ. The L-curve can be formed using any of t, Δ, and λ_Δ. They are interchangeable and used to parameterize the regularization problem to give points on the L-curve. These parameters are related to each other as follows:

$$\begin{aligned} t &= \lambda_\Delta + \delta U^T J \left(J^T J - \lambda_\Delta I\right)^{-1} J^T \delta U \\ \Delta^2 &= \delta U^T J \left(J^T J - \lambda_\Delta I\right)^{-2} J^T \delta U \\ \lambda_\Delta &= \lambda_1 \left(D\left(t\right)\right) \end{aligned} \tag{13}$$

More details regarding derivation of the above parameters are given in [4].

4. EXPERIMENTAL MEASURMENT SETUP

4.1. Measurements on Phantom

To validate the proposed approach, experiments were conducted on a cylindrical phantom of 10 cm height and 5 cm radius containing 48 circular stainless steel electrodes in three rings with each ring composed of 16 electrodes connected peripherally around the cylinder. The radius of each electrode was 0.3 cm, and the gap between electrodes was 1.35 cm. The phantom was filled with saline solution with 0.2 molar concentrations and connected to a newly designed EIT system. Our EIT system currently consists of 48 channels operating at multiple frequencies from 100 Hz–125 kHz that are continuously selectable. A digital signal processor (DSP) is used to control the operation of every

module. In order to convert measured raw data into amplitude and phase information, we have implemented a PC-based phase-sensitive detection which is used lock-in amplifiers.

The test objects were a metal rod 6 cm tall with diameters 1.5 cm and a plastic rod of the same height and diameter. These are high contrast objects when used in the saline solution background. Figure 1 depicts the objects and the overhead view of the electrode geometry.

The metal rod was 1.5 cm from electrode 1 and the plastic rod at the same depth near electrode 9. The adjacent current injection pattern and adjacent voltage measurement ('adjacent'-'adjacent') were implemented, and 2160 pairs of measurements in total were obtained. The frequency of the sine wave current was chosen for

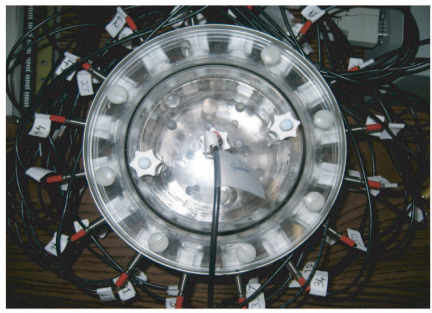

Figure 1. A cylindrical phantom with two test objects.

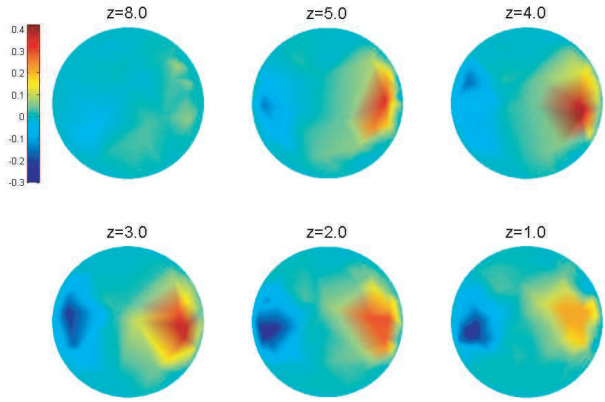

Figure 2. Reconstructed images with TRS at different height of phantom.

this test to be 125 kHz with a peak current of 4 mA. Two sets of measurements without and with test objects were performed. Each set of measurement was repeated fifty times for the purpose of standard deviation calculation. The calculated standard deviation was used as an estimation of measurement noise which was used to determine the stopping point for the CGLS approach.

In this study all three-dimensional reconstructed images are displayed as a series of two-dimensional image slices along the z-axis.

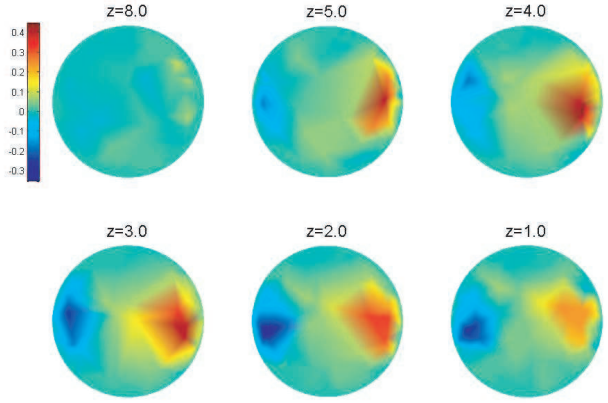

Figure 3. Reconstructed images with CGLS at different height of phantom.

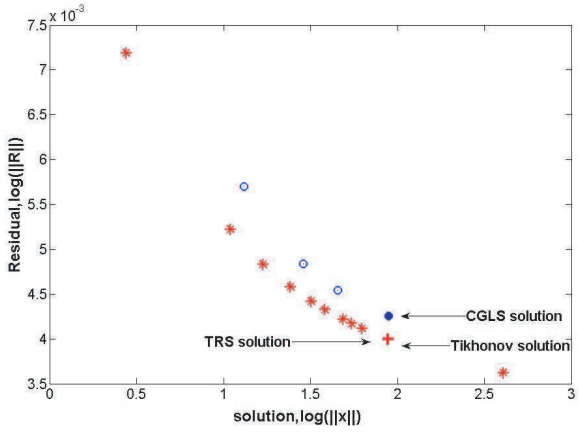

Figure 4. L-curve with TRS, CGLS, and best solution with Tikhonov.

4.2. Summary of Results

Figures 2–3 show the background-subtracted images for two TRS and CGLS methods. The metal rod appears as red while the plastic rod appears as blue. Figure 4 shows the different points on L-curve for both methods. The best possible solution that was obtained using Tikhonov method is also shown in the graph. Even though the curve is not strongly L-shaped, both horizontal and vertical parts are

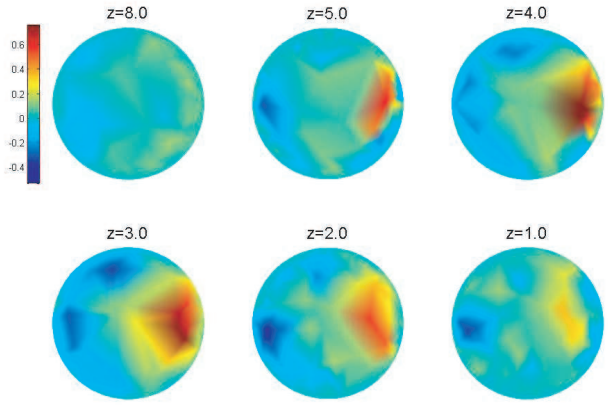

Figure 5. Reconstructed images with CGLS at 30% standard deviation.

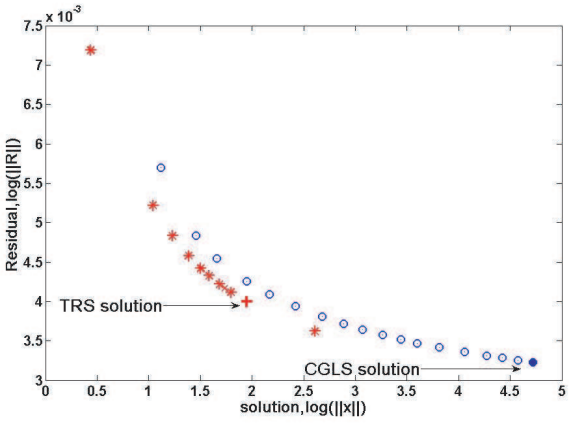

Figure 6. L-curve with TRS and CGLS at 30% standard deviation.

distinguishable. The TRS algorithm was able to locate the elbow, and this was close to the best solution by Tikhonov. Figures 5 shows the reconstructed images with CGLS where level of measurement noise was set to be 30% of calculated standard deviation. The norm of noise is used to terminate the iterations. Figure 6 shows the associated L-curve for CGLS.

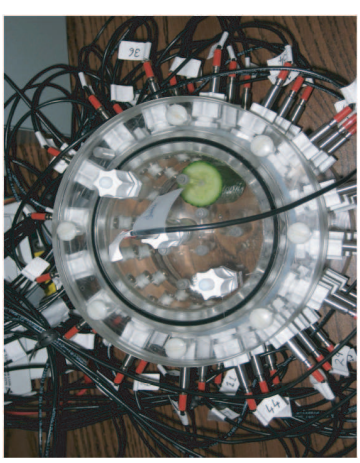

(a)

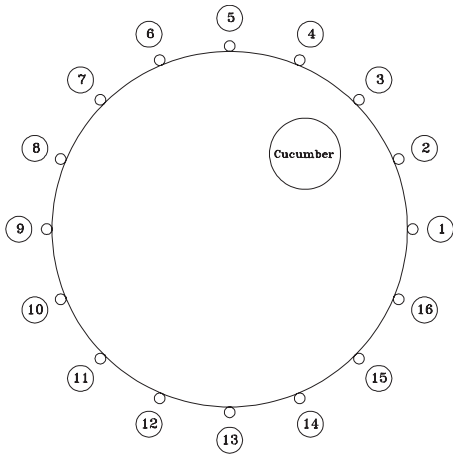

(b)

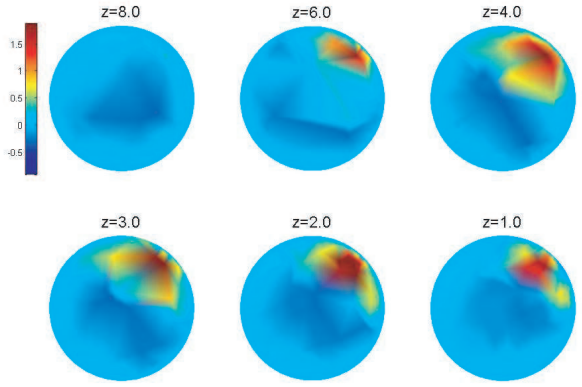

(c)

Figure 7. A piece of cucumber inside of saline tank, (b) position of cucumber relative to electrodes. (c) Reconstructed conductivity images of cucumber using TRS approach at 50 kHz. The cucumber was close to electrode 3.

In another experiment a piece of cucumber was inserted inside the phantom holder to evaluate the capability of TRS to reconstruct conductivity distribution of this test sample. Figure 7(a) illustrates the position of the cucumber inside the phantom holder. Figure 7(b) shows pictorially the placement of the cucumber near electrode 3. The TRS technique was used to reconstruct the conductivity variation of cucumber. Figure 7(c) shows the reconstructed images using the TRS technique. Cucumber was chosen as it is cellular structure should display impedances closer to what would be expected *in vivo*.

As can be seen, the TRS was able to build images based on correct position of the cucumber inside of phantom.

In another experiment two pieces of polyvinyl alcohol (PVA)-based cryogel (PVA-C) were suspended in phantom. A PVA-cryogel (or PVA-C) is a hydrogel manufactured by freezing up to (-20°C) and thawing ($+20$°C) in an aqueous PVA solution [12]. PVA-C gel phantom has been used to mimic organs and tissues in MR and ultrasound imaging studies [13]. In another work, we demonstrated that there are significant changes in the electrical properties of PVA-C that undergoes different doping [11]. Figures 7(a) and (b) illustrate the position of the two PVA-C inside the phantom. The top PVA-C is a pure polymer whereas the bottom one is a doped PVA with salt (1 Molar). Figure 7(c) depicts the reconstructed conductivity for these two pieces of PVA using TRS algorithm.

4.3. Discussion

The results show that the TRS was able to reconstruct images with the same performance as CGLS.

The two test objects were clearly distinguishable at correct positions in all different heights in Figure 2. The TRS algorithm was able to follow points on curvature and locate elbow as shown in Figure 4. The TRS selected solution (marked with +) was close to the best possible Tikhonov solution.

CGLS is known to be a fast and robust approach that has been used for regularization of ill-posed problems. It requires very low memory. The disadvantage of CGLS is the behaviour called *semiconvergence* which requires a knowledge of exactly when to terminate the iteration. The stopping criterion for CGLS is based on the discrepancy principle. It terminates when the residual is smaller than a predefined level. This level is set based on the norm of measurements noise. In this paper, the norm of measurements noise was estimated from standard deviation of repeated measurements. When the norm of noise was set equal to standard deviation of measurements the CGLS converges to the same result as TRS

(Figure 3). The CGLS results at each iteration were shown as circles above the TRS points in Figure 4.

The advantage of the TRS method compared to CGLS is that the former does not need any knowledge of noise for its process. As shown in Figures 5–6 when the norm of noise is estimated to be 30% of standard deviation of measurements, the CGLS terminated with larger number of iterations, and final result was much worse (Figure 5).

An additional advantage of the constrained least square approach in comparison to the Tikhonov method is that the physical properties of the problem could be used to estimate the norm of constraint Δ.

Trust region algorithms generate new iterates within a region near the current iteration point. This region is called the trust region. An example of trust region approach is the dogleg algorithm [14]. The

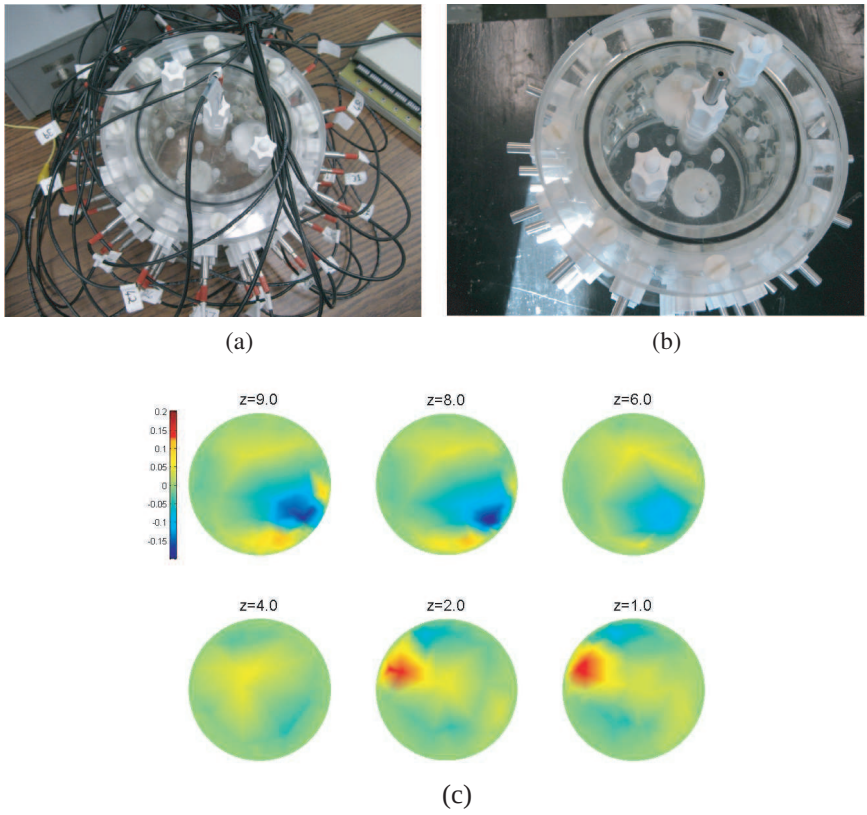

Figure 8. (a), (b) the actual position of two polyvinyl alcohol cryogel (PVA-C). The bottom PVA is doped with salt and top one is a pure PVA. (c) Reconstructed conductivity images of two PVA using TRS.

dogleg approximates a Levenberg-Marquardt approach within the trust region of the model function with a quadratic model. The iteration steps are calculated to minimize the *model function* inside the trust region. The success of the dogleg approach depends on a good choice of the regularization parameter.

It is shown that the Tikhnov regularization (Equation (4)) is equivalent to a special form of the trust-region subproblem with a quadratic constraint (Equation (3)). Therefore the trust region subproblem technique can be used to solve regularization problems of type (2), where instead of specifying a value for the Tikhonov parameter as required for (2), we need to define a bound on the norm of the desired solution.

5. CONCLUSIONS

In this study, a parameterized trust region technique was used to find the region of maximum curvature of the L-curve which was used to find the regularized solution.

The performance of TRS was compared to the conjugate gradients based method for solving the least-squares problems (CGLS). CGLS is an iterative method to solve linear equations and is a robust regularization technique for the case of very large problem.

However, comparing both CGLS and TRS solutions in Figures 2–3 we can see that both techniques reconstruct the same distribution. The TRS algorithm, though, does not require a specific value of the norm of the noise in its iteration process. The TRS algorithm has proven to be robust by converging towards solutions as it is shown in Figures 2–7.

REFERENCES

1. Eldén, L., "Algorithms for the regularization of ill-conditioned least squares problems," *BIT*, Vol. 17, 134–145, 1977.
2. Björck, A., "Numerical methods for least squares problems," *SIAM*, Philadelphia, 1996.
3. Rojas, M., "A large-scale trust-region approach to the regularization of discrete ill-posed problems," Ph.D. Thesis, Technical Report TR98-19, Department of Computational and Applied Mathematics, Rice University, Houston, 1998.
4. Grodzevich, O., "Regularization using a parameterized Trust-Region subproblem," M.Sc. Thesis, Department of Combinatorics and Optimization, University of Waterloo, Canada, 2004.

5. Hansen, P. C., "Analysis of discrete ill-posed problems by means of the L-curve," *SIAM Rev.*, Vol. 34, No. 2, 561–580, 1992.
6. Sorensen, D. C., "Minimization of a large-scale quadratic function subject to a spherical constraint," *SIAM Journal on Optimization*, Vol. 7, No. 1, 141–161, 1997.
7. Stern, R. J. and W. Hlkowicz, "Indefinite trust region subproblems and nonsymmetric eigenvalue perturbations," *SIAM Journal on Optimization*, Vol. 5, No. 2, 286–313, 1995.
8. Boone, K., D. Barber, and B. Brown, "Imaging with electricity: Report of the european concerted action on impedance tomography," *Journal of Medical Engineering & Technology*, Vol. 21, No. 4, 201–232, 1997.
9. Metherall, P., D. C. Barber, R. H. Smallwood, and B. H. Brown, "Three-dimensional electrical impedance tomography," *Nature*, Vol. 380, No. 6574, 509–512, 1996.
10. Vauhkonen, M., "Electrical impedance tomography and prior information," Thesis, Univeristy of Kuopio, 1997.
11. Goharian, M., G. R. Moran, K. Wilson, C. Seymour, A. Jegatheesan, M. Hill, R. T. Thompson, and G. Campbell, "Modifying the MRI, elastic stiffness and electrical properties of polyvinyl alcohol cryogel using irradiation," *Nucl. Instr. and Meth. B*, in press, 2007.
12. Mori, Y., H. Tokura, and M. Yoshikawa, "Properties of hydrogels synthesized by freezing and thawing aqueous polyvinyl alcohol solutions and their applications," *Journal of Materials Science*, Vol. 32, No. 2, 491–496, 1997.
13. Surry, K. J. M., H. J. B. Austin, A. Fenster, and T. M. Peters, "Poly (vinyl alcohol) cryogel phantoms for use in ultrasound and MR imaging," *Physics in Medicine and Biology*, Vol. 49, No. 24, 5529–5546, 2004.
14. Goharian, M., A. Jegatheesan, and G. R. Moran, "Dogleg trust-region application in electrical impedance tomography," *Physiol. Meas.*, Vol. 28, 555–572, 2007.
15. Soleimani, M., C. N. Mitchell, R. Banasiak, R. Wajman, and A. Adler, "Four-dimensional electrical capacitance tomography imaging using experimental data," *Progress In Electromagnetics Research*, PIER 90, 171–186, 2009.
16. Soleimani, M., "Simultaneous reconstruction of permeability and conductivity in magnetic induction tomography," *Journal of Electromagnetic Waves and Applications*, Vol. 23, Nos. 5–6, 785–798, 2009.

17. Zacharopoulos, A. and S. Arridge, "3D shape reconstruction in optical tomography using spherical harmonics and BEM," *Journal of Electromagnetic Waves and Applications*, Vol. 20, No. 13, 1827–1836, 2006.
18. Zhang, H., S. Y. Tan, and H. S. Tan, "A novel method for microwave breast cancer detection," *Progress In Electromagnetics Research*, PIER 83, 413–434, 2008.
19. Chen, G. P., W. B. Yu, Z. Q. Zhao, Z. P. Nie, and Q. H. Liu, "The prototype of microwave-induced thermo-acoustic tomography imaging by time reversal mirror," *Journal of Electromagnetic Waves and Applications*, Vol. 22, Nos. 11–12, 1565–1574, 2008.
20. Giamalaki, M. I., I. S. Karanasiou, and N. K. Uzunoglu, "Electromagnetic analysis of a non invasive microwave radiometry imaging system emphasizing on the focusing sensitivity optimization," *Progress In Electromagnetics Research*, PIER 90, 385–407, 2009.
21. Polydorides, N., "Linearization error in electrical impedance tomography," *Progress In Electromagnetics Research*, PIER 93, 323–337, 2009.